

Reconciling the Metallicity Distributions of Gamma-ray Burst, Damped Lyman- α , and Lyman-break Galaxies at $z \approx 3$

Johan P. U. Fynbo ¹, J. Xavier Prochaska ², Jesper Sommer-Larsen ^{3,1} Miroslava Dessauges-Zavadsky ⁴, Palle Møller ⁵

ABSTRACT

We test the hypothesis that the host galaxies of long-duration gamma-ray bursts (GRBs) as well as quasar-selected damped Ly α (DLA) systems are drawn from the population of UV-selected star-forming, high z galaxies (generally referred to as Lyman-break galaxies). Specifically, we compare the metallicity distributions of the GRB and DLA populations against simple models where these galaxies are drawn randomly from the distribution of star-forming galaxies according to their star-formation rate and HI cross-section respectively. We find that it is possible to match both observational distributions assuming very simple and constrained relations between luminosity, metallicity and HI sizes. The simple model can be tested by observing the luminosity distribution of GRB host galaxies and by measuring the luminosity and impact parameters of DLA selected galaxies as a function of metallicity. Our results support the expectation that GRB and DLA samples, in contrast with magnitude limited surveys, provide an almost complete census of $z \approx 3$ star-forming galaxies that are not heavily obscured.

Subject headings: gamma-rays: bursts – interstellar medium

¹Dark Cosmology Centre, Niels Bohr Institute, University of Copenhagen; Juliane Maries Vej 30, 2100 Copenhagen O, Denmark; jfynbo@dark-cosmology.dk

²Department of Astronomy and Astrophysics, UCO/Lick Observatory; University of California, 1156 High Street, Santa Cruz, CA 95064; xavier@ucolick.org

³Excellence Cluster Universe, Technische Universität München; Boltzmannstr. 2, D-85748 Garching, Germany

⁴Observatoire de Genève, 51 Ch. des Maillettes, 1290 Sauverny, Switzerland

⁵European Southern Observatory, Karl-Schwarzschild-strasse 2, D-85748 Garching bei München

1. Introduction

The past 10 years has marked the emergence of extensive observational analysis of high redshift ($z > 2$) galaxies. This remarkable and rapid advance was inspired by new technologies in space and ground-base facilities for deep imaging, clever approaches to target selection, and the arrival of 10 m class ground-based telescopes for spectroscopic confirmation. A plethora of classes are now surveyed, each named for the observational technique that selects the galaxies: the Ly α emitters (Hu et al. 1998), the Lyman break galaxies (LBGs, Steidel et al. 2003), sub-mm galaxies (e.g., Chapman et al. 2005), distant red galaxies (van Dokkum et al. 2006), damped Ly α (DLA) systems (Wolfe et al. 2005), extremely red objects (Cimatti et al. 2003), long-duration γ -ray burst (GRB) host galaxies (e.g., Fruchter et al. 2006), Mg II absorbers, radio galaxies (Miley & De Breuck 2008), quasar (QSO) host galaxies, etc. Large, dedicated surveys have identified in some cases thousands of these galaxies providing a direct view into the processes of galaxy formation in the young universe.

Because of the significant differences in the sample selection of high z galaxies, there has been a tendency by observers to treat each population separately and/or contrast the populations. However, the various populations will overlap to some extent and it is important to understand how (see also Adelberger & Steidel 2000; Møller et al. 2002; Fynbo et al. 2003; Reddy et al. 2005).

Of the various galactic populations discovered at $z > 2$ to date, only two offer the opportunity to study the interstellar medium at a precision comparable to the Galaxy and its nearest neighbors: the damped Ly α systems intervening quasar sightlines (QSO-DLA) and the host galaxies of GRBs which exhibit bright afterglows (GRB-DLA¹). These galaxies are characterized by a bright background source which probes the gas along the sightline to Earth. In the case of QSO-DLA it is the background QSO while for GRB-DLA it is the afterglow of the GRB located within the host galaxy. Hence, the GRB-DLA will not probe the full line-of-sight through the host. The gas in the ISM imprints signatures of the total H I column density, the metal content, the ionization state, the velocity fields, and the molecular fraction along the line-of-sight. Because the galaxies are identified in absorption, there is no formal magnitude limit for the associated stellar populations. In this respect, they may trace a large dynamic range in stellar mass, morphology, star formation rate, etc.

¹A small fraction of these GRB afterglow spectra have H I column densities in the host galaxy that are below the standard DLA definition $N_{\text{HI}} = 2 \times 10^{20} \text{ cm}^{-2}$ (Jakobsson et al. 2006a; Dessauges-Zavadsky al. 2008, in prep). These GRB-LLS will not be considered here. Similarly, the QSO absorption line systems with H I column densities between 10^{17} and $2 \times 10^{20} \text{ cm}^{-2}$ (the empirical threshold for the DLAs) will not be considered here.

The connection between long-duration GRBs and star-forming galaxies has been empirically established. At large redshift, there is an exclusive coincidence of GRBs with actively star-forming galaxies (e.g., Hogg & Fruchter 1999; Bloom et al. 2002; Fruchter et al. 2006), the majority of which show elevated specific star-formation rates (Christensen et al. 2004). At low z , there is a direct link between GRBs and massive stars via the detection of spatially and temporally coinciding core-collapse supernovae (Hjorth et al. 2003; Stanek et al. 2003, but see also Fynbo et al. 2006). Furthermore, GRBs are in some cases found in Wolf-Rayet galaxies (Hammer *et al.* 2006), which further strengthens the link between GRBs and massive star-formation. The simplest hypothesis, therefore, is that these galaxies uniformly sample high z galaxies according to star-formation rate, i.e. $f_{GRB}(L) \propto SFR(L)\phi(L)$, where $\phi(L)$ is the luminosity function.

The link between QSO-DLA and star-forming galaxies is less direct, primarily because the bright background quasar precludes the easy detection of stellar light. Nevertheless, the presence of heavy metals in all QSO-DLAs (and dust in the majority) indicates at least prior star-formation (Prochaska et al. 2003). Furthermore, the observation of C II* absorption suggests heating of the ISM by far-UV photons from ongoing star-formation in at least half of the sample (Wolfe et al. 2003, 2004). Finally, a handful of QSO-DLA have been detected in emission and exhibit properties similar to low luminosity LBGs (Møller et al. 2002). In contrast to the GRB-DLA, however, the QSO-DLA are selected according to their covering fraction on the sky, i.e. the probability of detection is the convolution of the H I cross-section with the luminosity function: $f_{DLA}(L) \propto \sigma_{HI}(L)\phi(L)$. While both populations of DLAs may be drawn from the full sample of star-forming galaxies, their distribution functions would only be the same if $\sigma_{HI}(L) \propto SFR(L)$ (see also Chen et al. 2000).

In this paper, we will test these ideas by comparing the observed metallicity distributions of QSO-DLA and GRB-DLA with simple predictions based on empirical measurements of star-forming galaxies at $z = 3$. Specifically, we combine the luminosity function of UV-selected galaxies (LBGs), a metallicity/luminosity relation, and a simple prescription for the radial distribution of H I gas with luminosity to predict the metallicity distributions of the QSO-DLA and GRB-DLA. We then compare these models with current observation to test this general picture. This analysis is similar in spirit to the studies of Fynbo et al. (1999) who combined the LBG luminosity function with a Holmberg relation for σ_{HI} to predict the luminosities and impact parameters of QSO-DLA galaxies, Jakobsson et al. (2005) who compared the luminosity distribution function of GRB host galaxies with the LBG luminosity function, and Chen et al. (2005) and Zwaan et al. (2005) who reconciled the properties of local galaxies with the QSO-DLA cross-section and metal abundances.

The paper is structured in the following way: In Sect. 2 we describe our methodology,

in Sect. 3 our results and in Sect. 4 a discussion of the results obtained and the uncertainties behind the analysis.

Throughout the paper we assume a cosmology with $\Omega_\Lambda = 0.70$, $\Omega_m = 0.30$, $h = 0.7$.

2. Methodology and Analysis

The goal of this paper is to test the hypothesis that galaxies hosting QSO-DLA and GRB-DLA are drawn from the (same) general population of star-forming galaxies at high z , according to H I cross-section and SFR respectively. We will approach this hypothesis in a simple, empirical fashion.

Our observational constraint will be the metallicity distribution function of the two populations shown in Fig. 1. The metallicity values are measured in the same manner for these DLAs: the H I column density is derived from a Voigt profile analysis of the Ly α transition and the metal column density is estimated from low-ion transitions of non-refractory (or mildly refractory) elements, e.g. S, Si and Zn. In the following, we will adopt the statistical samples compiled by Prochaska et al. (2003) and Prochaska et al. (2007) for the QSO-DLA and GRB-DLA respectively. The redshift range for both samples is approximately 2–4. We emphasize that nebular measurements of local and distant galaxies are generally in good agreement with the ISM values (Bowen et al. 2005; Schulte-Ladbeck et al. 2005; Pettini et al. 2002). For the GRB-DLA, this is a reasonable expectation because one probes gas surrounding the star-forming region that hosted the GRB event (Prochaska et al. 2006). For the QSO-DLA, however, one expects the ISM probed by these sightlines to be at systematically larger impact parameter, i.e. away from central star-forming regions. If a radial metallicity gradient exists in high z galaxies, then the QSO-DLA would give systematically lower metallicity values than the nebular measurements. We address this effect in the following analysis. Finally, we note that approximately half of the GRB-DLA metallicity measurements are lower limits because of line saturation. Also, the GRB-DLA sample is both heterogeneous (including GRBs from a range of satellites) and biased towards GRBs with bright optical afterglows. In Sect. 4.1 we further discuss the issue of bias.

In Fig. 2 and Fig. 3 we illustrate our model with a number of schematic figures. Fig. 2 shows a small subfield from the Hubble Deep Field (HDF) North (Williams et al. 1996). We have here overplotted randomly inclined HI disks with sizes as in our model on galaxies with photometric redshifts in the range 2.8–3.2. For two of the galaxies, we also show the radial metallicity profile as assumed in our model. The lower panel in Fig. 3 shows the cumulative distribution function for observed R-band magnitude for GRB host galaxies and QSO-DLA

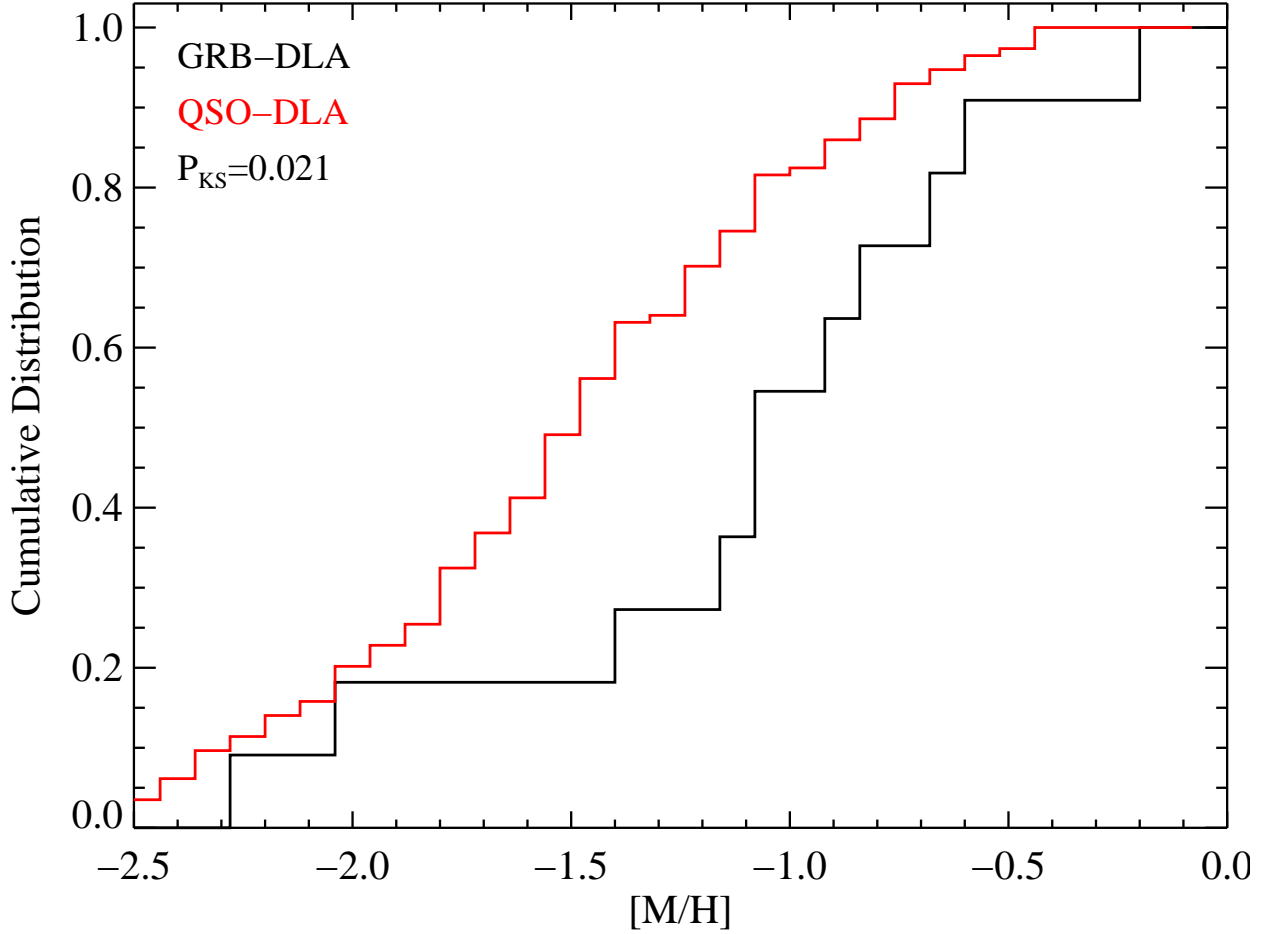


Fig. 1.— The histograms show the cumulative distribution of QSO-DLA and GRB-DLA metallicities in the statistical samples compiled by Prochaska et al. (2003) and Prochaska et al. (2007). As seen, the GRB-DLA metallicities are systematically higher than the QSO-DLA metallicities.

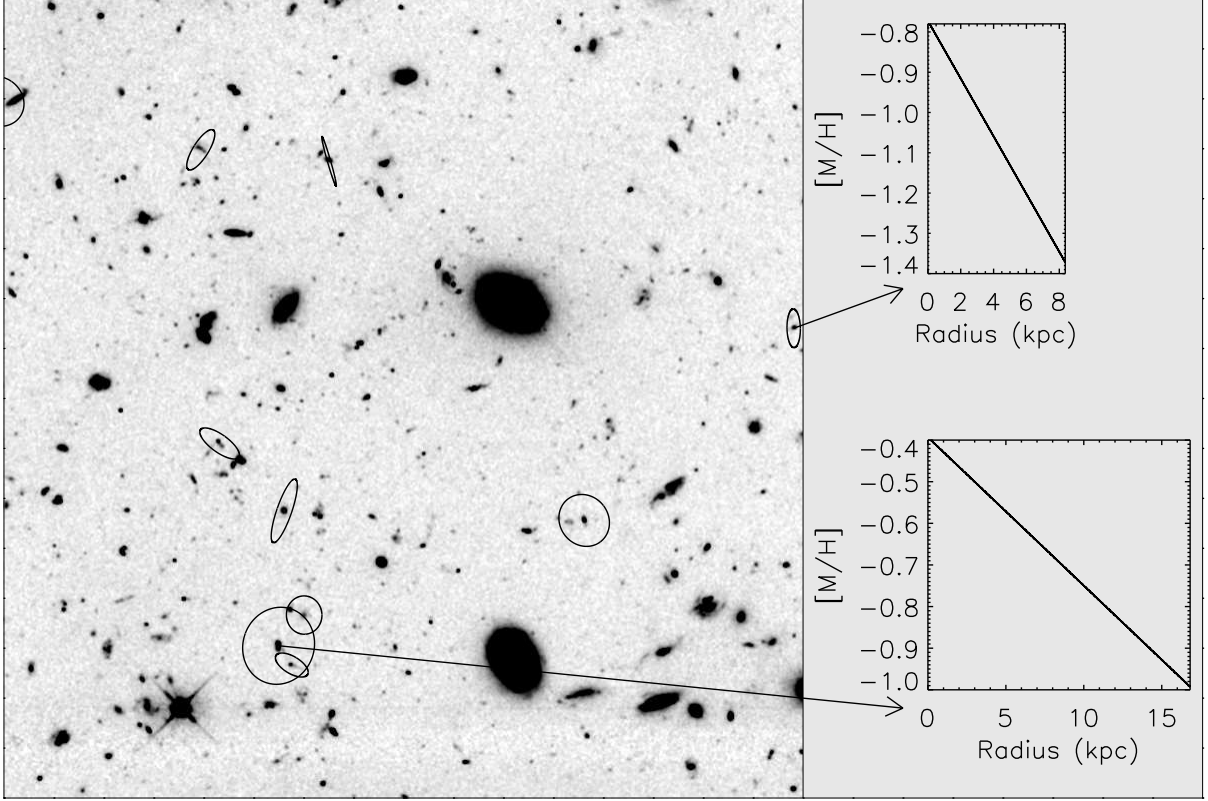


Fig. 2.— A subfield from the HDF North R -band image. We have selected LBGs with redshift between 2.8 and 3.2 from the catalog of photometric redshifts of Fernández-Soto et al. (1999). Over-plotted on each LBGs is the extent of a randomly inclined HI disk with a radius given in the text. Note that the majority of the total QSO-DLA absorption cross-section is caused by fainter galaxies than those shown here. On the right we show the radial metallicity profile from the centre to R_{HI} in our model for two of the galaxies.

galaxies. It is seen that GRB hosts are expected to be brighter than QSO-DLA galaxies on average. The middle panel shows the impact parameter distribution for QSO-DLA galaxies in our model. In particular it is seen that the highest metallicity QSO-DLA will be the brightest and have the largest impact parameters. The top panel shows the metallicity distribution for QSO-DLA (at the QSO-sightline) and GRB host galaxies in our model.

2.1. Luminosity Function

Our model is guided by empirical observations of star-forming galaxies. In the following, we assume that the UV-selected sample of $z \sim 3$ galaxies (i.e. LBGs) accurately traces the complete sample of star-forming galaxies (e.g., Adelberger & Steidel 2000). The key caveat is that UV-selected samples are biased against extremely dusty galaxies (e.g., Hughes et al. 1998; van Dokkum et al. 2006). This bias should, however, be a minor effect for galaxies with low SFR where dust extinction is largely negligible. To this extent, we expect the number density of galaxies with low SFR is well described by the faint end of the UV luminosity function determined from LBG samples. At very large SFR, however, the UV-selected sample may be incomplete and one must at least consider contributions from populations that better trace dust enshrouded, star-forming galaxies (e.g. sub-mm sources, extremely red objects). We will argue below, however, that the dust bias of UV-selected samples has a minor effect on our conclusions.

We will adopt the UV luminosity function measured by Reddy et al. (2008) which provides the largest compilation of spectroscopically confirmed $z \sim 3$ LBGs to date. The luminosity function for these galaxies measured at rest-frame 1700\AA is well approximated by a Schechter function,

$$\phi(L_{1700}) = \phi_*(L_{1700}/L_*)^\alpha \exp(-L_{1700}/L_*) \quad (1)$$

with a value of α in the range -1.6 to -2.0 and $M_* = -20.84 \pm 0.12$. Regarding our analysis, the most important characteristic of this luminosity function is its very steep faint-end slope. Even with $\alpha = -1.6$, galaxies with $L > L_*$ contribute only $\approx 10\%$ of the total UV light. It is not surprising, therefore, that most magnitude-limited surveys of high z galaxies trace only the ‘tip of the iceberg’ of the full galactic population (see also the discussion in Sommer-Larsen & Fynbo 2008). Note that while the bright end has an exponential cutoff, there is no empirical constraint that sets the faint-end limit, L_{min} . This is even true in the local universe where one can attain very sensitive limits (Jerjen et al. 2004). Baldry et al. (2005), for example, have measured the local u-band luminosity function and find no break in the shape of the faint-end slope down to their detection limit of $0.016L_*$. Similarly, Blanton et

al. (2005) examined extremely faint galaxies in the Sloan Digital Sky Survey (SDSS) and identified an upturn in the faint-end slope towards $\alpha = -1.5$ at $M > -18$. Hence, there is no evidence from the local Universe that the faint end turns over. On the contrary, it seems to have an increasing slope with the faintest star-forming dwarfs having luminosities around $0.0001 L_*$ (Mateo 1998).

At redshifts $z \approx 3$, GRB hosts are among the faintest known galaxies. The most striking case is the $z = 3.20$ (Hjorth et al. 2003) GRB 020124 for which Berger et al. (2002) placed a limit of $R = 29.5$ on the magnitude of the host galaxy. This corresponds to $L < 0.01 L_*$. Recently, an indirect probe of the $z = 3$ luminosity function has been carried out via very faint Ly α emitters (Rauch et al. 2007). This study finds that a Schechter function with $\alpha = -1.7$ provides a good fit to about $0.025 L_*$. There is some indication of a flattening of the slope between 0.025 and $0.01 L_*$. In the following, we will consider values ranging from $L_{min} = 0.1$ to $10^{-5} L_*$.

2.2. Metallicity-Luminosity Relation

To convert the luminosity function into a metallicity distribution for comparison with the GRB and DLA populations, we must adopt a metallicity/luminosity relation. In the local universe, metallicity traces luminosity in low mass (dwarf) galaxies and ‘saturates’ in brighter galaxies (Dekel & Woo 2003; Tremonti et al. 2004). Similar trends have been found for smaller samples of intermediate and high z galaxies (Kobulnicky & Kewley 2004; Møller et al. 2004; Savaglio et al. 2005; Erb et al. 2006). Guided by these empirical trends, we will assume a metallicity/luminosity relation of the form

$$Z = Z_* \left(\frac{L}{L_*} \right)^\beta \quad (2)$$

This relation has two parameters: a normalization Z_* and a slope β . In the following we will assume $Z_* = Z_\odot/2$ which is supported by the handful of precision LBG metallicity measurements to date (e.g. Pettini et al. 2001). We adopt $\beta = 0.2$ for the slope which lies central to the various estimates from local and high z analyses (Tremonti et al. 2004; Erb et al. 2006; Ledoux et al. 2006; Prochaska et al. 2007). It is also supported by numerical simulation of $z = 3$ galaxies (Fig. 4). Although our relation does not level off at $L > L_*$, our conclusions are insensitive to super- L_* galaxies.

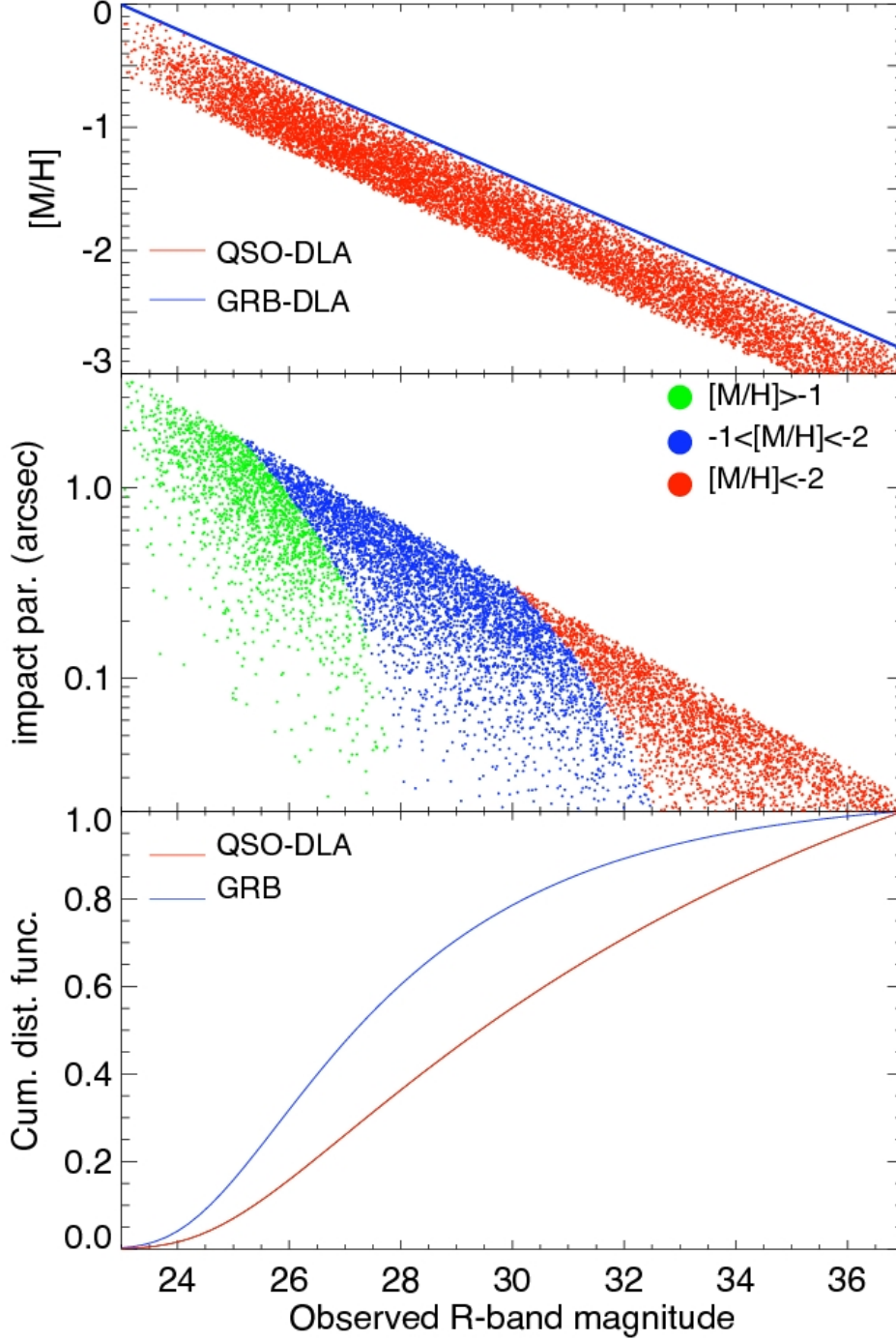


Fig. 3.— Simulated distributions of luminosity, impact parameter and metallicity (from bottom to top) for QSO-DLA and GRB galaxies at $z = 3$ in our model. Here we have used $\alpha = -1.7$, $\beta = 0.2$, $L_{min} = 10^{-4}L^*$, $t = 0.4$, and $\gamma^* = -0.03$. In the top panel, QSO-DLA have lower metallicities than GRB hosts at a given R-band magnitude due to the metallicity gradients. In the middle panel impact parameters are lower for fainter QSO-DLA galaxies due to the Holmberg relation and low metallicity QSO-DLA have lower impact parameters due to the luminosity-metallicity relation and the Holmberg relation. In the lower panel QSO-DLA galaxies are fainter than GRB hosts as for $t = 0.4$ the selection function for QSO-DLA weights fainter galaxies more than the selection function for GRBs.

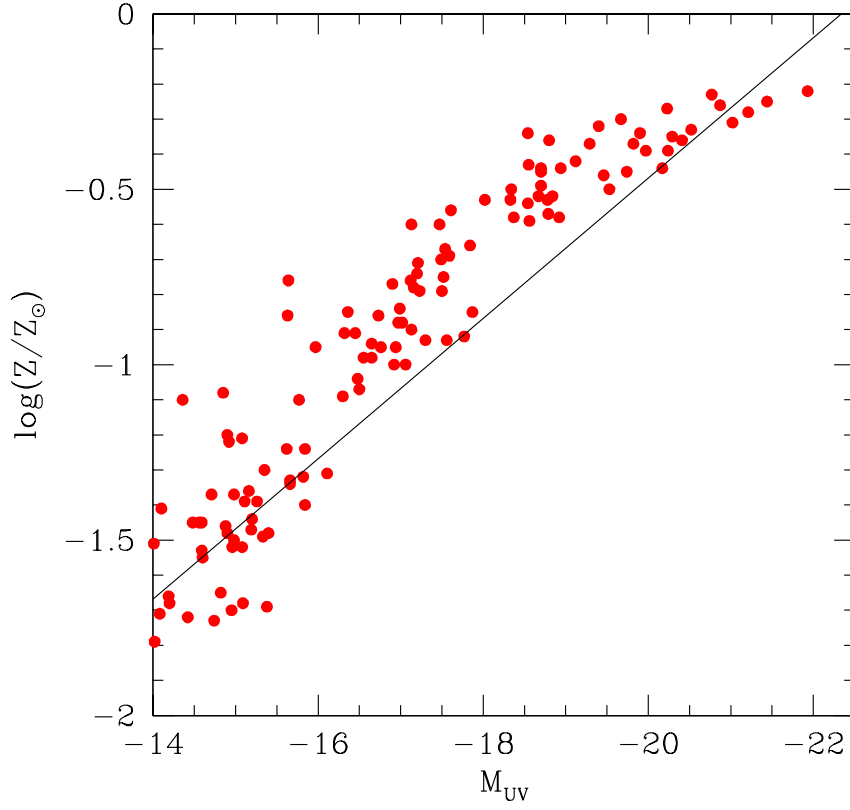


Fig. 4.— The UV luminosity-metallicity relation from the numerical simulations of $z = 3$ galaxies (from the simulations discussed in Sommer-Larsen & Fynbo 2008). A slope of $\beta = 0.2$ matches the distribution for simulated galaxies reasonably well.

2.3. Modeling the H I and Metal Distributions

To test our hypothesis with QSO-DLA, we must introduce a relation between H I cross-section and luminosity, $\sigma_{HI}(L)$. Here we adopt a Holmberg relation of the form

$$R_{HI}/R_* = (L/L_*)^t \quad (3)$$

where $t = 0.4$ locally (see, e.g., Wolfe et al. 2005, and discussion therein). For a direct measurement of t for QSO-DLA see also Chen & Lanzetta (2003). The value of R_* is fixed so as to reproduce the observed line density of DLAs $dn/dz(z = 3) = 0.25$ (Prochaska, Herbert-Fort & Wolfe 2005). For randomly inclined disks the relation between dn/dz and R_* can be derived for the assumed cosmology following Wolfe et al. (1986):

$$\frac{dn}{dz} = (1+z)^3 \frac{dr_{prop}}{dz} \int_{L_{min}}^{\infty} \phi(L) \pi R_{HI}^2 / 2 dL \quad (4)$$

where ϕ is the luminosity function and r_{prop} is the proper radial coordinate. Hence, R_* is given by

$$R_* = \sqrt{\frac{dn}{dz} \frac{2H_0}{\pi c(1+z)^2 I} \sqrt{(1+z)^2(\Omega_m z + 1) - \Omega_\Lambda z(z+2)}} \quad (5)$$

where $I = \int_{L_{min}}^{\infty} \phi_*(L/L_*)^{\alpha+2t} \exp(-L/L_*) dL$ and H_0 is the Hubble parameter.

While the GRB-DLA yield metallicity measurements of the gas near star-forming regions, the cross-section to QSO-DLA is maximal at large impact parameters and these sight-lines will show systematically lower metallicity than the inner SF regions if a metallicity gradient is in place at high z . We will allow for this effect in our model by assuming a metallicity gradient

$$\gamma = d \log Z / dR \quad (6)$$

In the local group values for γ measured for the Galaxy and M33 are -0.07 and -0.05 dex kpc^{-1} (Smartt et al. 1997; Magrini et al. 2007). Lower absolute values for γ are found for other galaxies, e.g. $\gamma = -0.02$ dex kpc^{-1} for M51 (Bresolin et al. 2004). In our model we will follow the work Boissier & Prantzos (2001) and let γ depend on luminosity according to the relation:

$$\gamma = \gamma_* R_* / R_{HI} \quad (7)$$

We will consider γ_* values ranging from -0.01 to -0.07 dex kpc^{-1} .

3. Results

In Fig. 1 we plot the cumulative metallicity distribution functions for QSO-DLA and GRB-DLA in the statistical samples compiled by Prochaska et al. (2003) and Prochaska

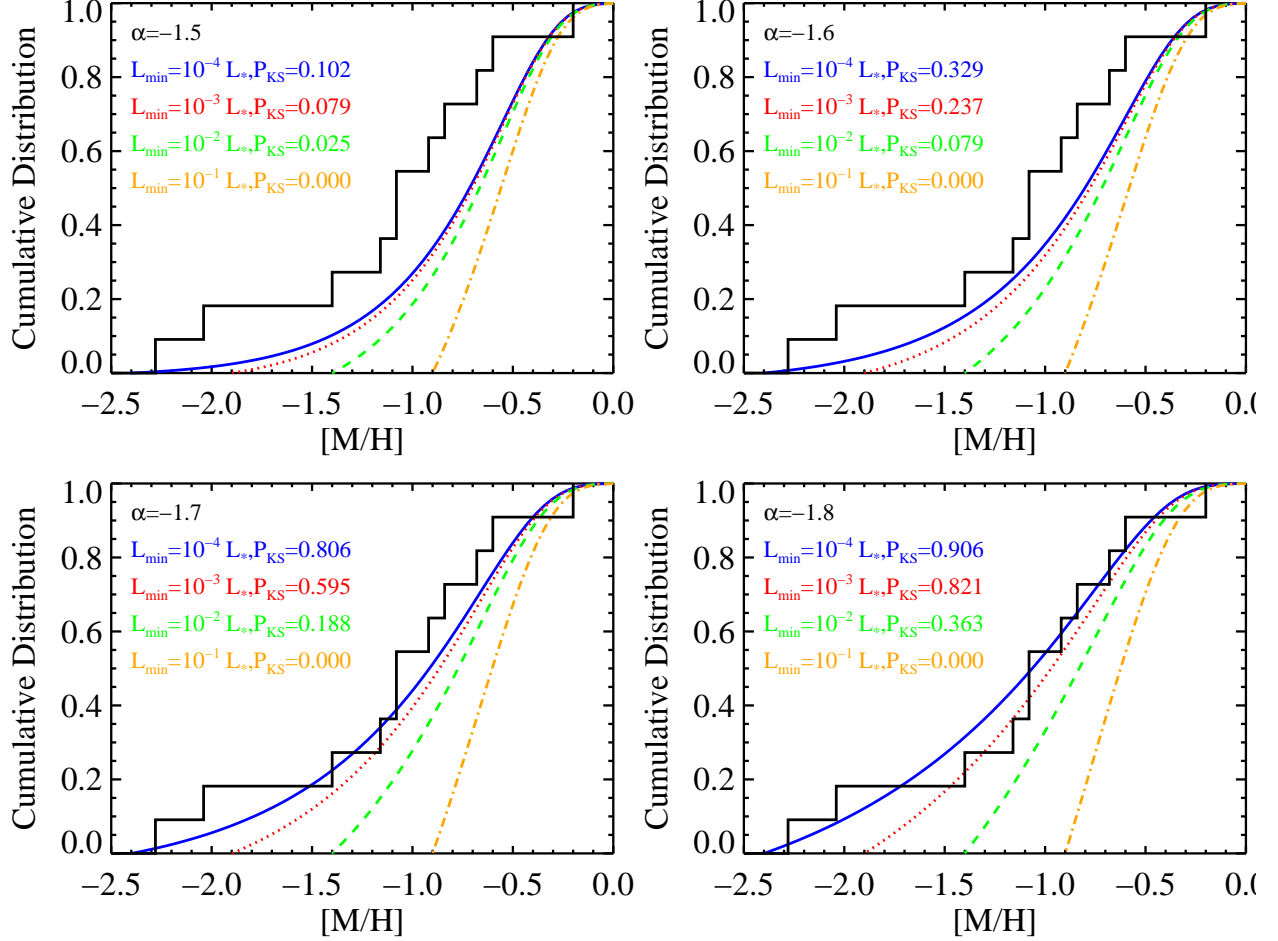


Fig. 5.— The black histograms compare the observed cumulative distribution of GRB-DLA metallicities against predictions from a series of simple models where one assumes that GRB host galaxies are drawn according to current SFR from the complete set of star-forming galaxies. The four panels show models assuming faint-end slopes for the luminosity function ranging from $\alpha = -1.5$ to $\alpha = -1.8$. For each assumed value of α we plot the model predictions for an assumed lower-limit to the luminosity of star-forming galaxies L_{\min} ranging from $10^{-1}L_*$ (orange dash-dot line) to $10^{-4}L_*$ (blue solid line) in steps of factors of 10. For each model we derive the probability of a KS test comparing the model to the data and find good agreement for the majority of parameter space explored. Models with $\alpha > -1.6$ and/or $L_{\min} > 0.01L_*$ are disfavored by the data.

et al. (2007). For this figure and the following analyses, we have incremented the six GRB-DLA lower limits by +0.2 dex. This is a conservative correction; the true value could be significantly higher (Prochaska 2006). It is evident that the GRB-DLA metallicities are higher than the QSO-DLA metallicities (see also Savaglio 2006, Fynbo et al. 2006b). In our model, this offset arises naturally from two effects: *i*) the generally higher impact parameters of QSO-DLA relative to GRB-DLA, and *ii*) the fact that QSO-DLA are cross-section selected whereas GRB-DLA are selected from SFR per luminosity bin. As long as the Holmberg parameter $t < 0.5$ (eqn. 3) this will make GRB selected galaxies brighter and hence more metal rich than QSO-DLA selected galaxies on average.

We can now test the hypothesis that GRB-DLA are uniformly drawn from the luminosity function of star-forming galaxies weighted by current SFR, i.e. $f_{GRB}(L) \propto \text{SFR}(L)\phi(L)$. To weight by SFR, we assume that $\text{SFR}(L) \propto L_{1700}$, i.e. the far-UV luminosity is an excellent proxy for the SFR (see also Kennicutt 1998). Using equation 2 to convert the SFR-weighted luminosity function to metallicity, we derive the cumulative distributions shown in Fig. 5. It is evident that many of the models are in agreement with the observed distribution. We present the P_{KS} values from a one-sided Kolmogorov-Smirnov test which represent the probability that the null hypothesis of the observational sample having been drawn from the model is ruled out. We conclude that the metallicity distribution of GRB-DLA at $z \sim 3$ is consistent with the prediction that GRBs directly trace the star-formation rate and that the host metallicities follow a luminosity-metallicity relation. We also conclude that models with $\alpha > -1.6$ and/or $L_{min} > 0.01L_*$ are disfavored by the data.

For the QSO-DLA, we draw galaxies randomly using $\sigma_{HI}(L)$ as the weighting factor, i.e. $f_{DLA}(L) \propto \sigma_{HI}(L)\phi(L)$. We randomly associate an impact parameter to the galaxy using again cross-section as weight. Finally we associate a metallicity to the sightline using eq. 2 and eq. 6. In Fig. 6 we plot models of the QSO-DLA metallicity distribution. Here we assume $\alpha = -1.7$ and $L_{min} = 0.0001L_*$ for all fits and vary the values of t and γ_* . The best model, which is consistent with the data, has $t = 0.4$ and $\gamma_* = -0.03 \text{ dex kpc}^{-1}$. We provide the results for a more exhaustive parameter search in Table 1.

Table 1. RESULTS FOR QSO-DLA. Full table only to be included in the electronic version.

t	α	L_{min} (L_*)	γ_* (dex kpc $^{-1}$)	P_{KS}^a
0.2	-1.6	10^{-0}	-0.01	< 0.001
0.2	-1.6	10^{-0}	-0.02	< 0.001
0.2	-1.6	10^{-0}	-0.03	< 0.001
0.2	-1.6	10^{-0}	-0.04	< 0.001
0.2	-1.6	10^{-0}	-0.05	0.003
0.2	-1.6	10^{-0}	-0.06	0.062
0.2	-1.6	10^{-0}	-0.07	0.002
0.2	-1.6	10^{-1}	-0.01	< 0.001
0.2	-1.6	10^{-1}	-0.02	< 0.001
0.2	-1.6	10^{-1}	-0.03	0.008
0.2	-1.6	10^{-1}	-0.04	0.083
0.2	-1.6	10^{-1}	-0.05	0.007
0.2	-1.6	10^{-1}	-0.06	< 0.001
0.2	-1.6	10^{-1}	-0.07	< 0.001
0.2	-1.6	10^{-2}	-0.01	< 0.001
0.2	-1.6	10^{-2}	-0.02	< 0.001
0.2	-1.6	10^{-2}	-0.03	< 0.001
0.2	-1.6	10^{-2}	-0.04	< 0.001
0.2	-1.6	10^{-2}	-0.05	< 0.001
0.2	-1.6	10^{-2}	-0.06	< 0.001
0.2	-1.6	10^{-2}	-0.07	< 0.001
0.2	-1.7	10^{-0}	-0.01	< 0.001
0.2	-1.7	10^{-0}	-0.02	< 0.001
0.2	-1.7	10^{-0}	-0.03	< 0.001
0.2	-1.7	10^{-0}	-0.04	< 0.001
0.2	-1.7	10^{-0}	-0.05	< 0.001
0.2	-1.7	10^{-0}	-0.06	0.020
0.2	-1.7	10^{-0}	-0.07	0.010
0.2	-1.7	10^{-1}	-0.01	< 0.001
0.2	-1.7	10^{-1}	-0.02	< 0.001
0.2	-1.7	10^{-1}	-0.03	0.001
0.2	-1.7	10^{-1}	-0.04	0.012
0.2	-1.7	10^{-1}	-0.05	0.003
0.2	-1.7	10^{-1}	-0.06	< 0.001
0.2	-1.7	10^{-1}	-0.07	< 0.001
0.2	-1.7	10^{-2}	-0.01	< 0.001

Table 1—Continued

t	α	L_{min} (L_*)	γ_* (dex kpc $^{-1}$)	P_{KS}^a
0.2	−1.7	10^{-2}	−0.02	< 0.001
0.2	−1.7	10^{-2}	−0.03	< 0.001
0.2	−1.7	10^{-2}	−0.04	< 0.001
0.2	−1.7	10^{-2}	−0.05	< 0.001
0.2	−1.7	10^{-2}	−0.06	< 0.001
0.2	−1.7	10^{-2}	−0.07	< 0.001
0.2	−1.8	10^{-0}	−0.01	< 0.001
0.2	−1.8	10^{-0}	−0.02	< 0.001
0.2	−1.8	10^{-0}	−0.03	< 0.001
0.2	−1.8	10^{-0}	−0.04	< 0.001
0.2	−1.8	10^{-0}	−0.05	< 0.001
0.2	−1.8	10^{-0}	−0.06	< 0.001
0.2	−1.8	10^{-0}	−0.07	0.023
0.2	−1.8	10^{-1}	−0.01	< 0.001
0.2	−1.8	10^{-1}	−0.02	< 0.001
0.2	−1.8	10^{-1}	−0.03	< 0.001
0.2	−1.8	10^{-1}	−0.04	0.003
0.2	−1.8	10^{-1}	−0.05	< 0.001
0.2	−1.8	10^{-1}	−0.06	< 0.001
0.2	−1.8	10^{-1}	−0.07	< 0.001
0.2	−1.8	10^{-2}	−0.01	< 0.001
0.2	−1.8	10^{-2}	−0.02	< 0.001
0.2	−1.8	10^{-2}	−0.03	< 0.001
0.2	−1.8	10^{-2}	−0.04	< 0.001
0.2	−1.8	10^{-2}	−0.05	< 0.001
0.2	−1.8	10^{-2}	−0.06	< 0.001
0.2	−1.8	10^{-2}	−0.07	< 0.001
0.3	−1.6	10^{-0}	−0.01	< 0.001
0.3	−1.6	10^{-0}	−0.02	< 0.001
0.3	−1.6	10^{-0}	−0.03	< 0.001
0.3	−1.6	10^{-0}	−0.04	0.002
0.3	−1.6	10^{-0}	−0.05	0.231
0.3	−1.6	10^{-0}	−0.06	0.009
0.3	−1.6	10^{-0}	−0.07	< 0.001
0.3	−1.6	10^{-1}	−0.01	< 0.001
0.3	−1.6	10^{-1}	−0.02	< 0.001

Table 1—Continued

t	α	L_{min} (L_*)	γ_* (dex kpc $^{-1}$)	P_{KS}^a
0.3	−1.6	10^{-1}	−0.03	0.090
0.3	−1.6	10^{-1}	−0.04	0.429
0.3	−1.6	10^{-1}	−0.05	0.018
0.3	−1.6	10^{-1}	−0.06	< 0.001
0.3	−1.6	10^{-1}	−0.07	< 0.001
0.3	−1.6	10^{-2}	−0.01	0.144
0.3	−1.6	10^{-2}	−0.02	0.130
0.3	−1.6	10^{-2}	−0.03	0.006
0.3	−1.6	10^{-2}	−0.04	< 0.001
0.3	−1.6	10^{-2}	−0.05	< 0.001
0.3	−1.6	10^{-2}	−0.06	< 0.001
0.3	−1.6	10^{-2}	−0.07	< 0.001
0.3	−1.7	10^{-0}	−0.01	< 0.001
0.3	−1.7	10^{-0}	−0.02	< 0.001
0.3	−1.7	10^{-0}	−0.03	< 0.001
0.3	−1.7	10^{-0}	−0.04	< 0.001
0.3	−1.7	10^{-0}	−0.05	0.063
0.3	−1.7	10^{-0}	−0.06	0.030
0.3	−1.7	10^{-0}	−0.07	< 0.001
0.3	−1.7	10^{-1}	−0.01	< 0.001
0.3	−1.7	10^{-1}	−0.02	< 0.001
0.3	−1.7	10^{-1}	−0.03	0.024
0.3	−1.7	10^{-1}	−0.04	0.172
0.3	−1.7	10^{-1}	−0.05	0.016
0.3	−1.7	10^{-1}	−0.06	< 0.001
0.3	−1.7	10^{-1}	−0.07	< 0.001
0.3	−1.7	10^{-2}	−0.01	0.019
0.3	−1.7	10^{-2}	−0.02	< 0.001
0.3	−1.7	10^{-2}	−0.03	< 0.001
0.3	−1.7	10^{-2}	−0.04	< 0.001
0.3	−1.7	10^{-2}	−0.05	< 0.001
0.3	−1.7	10^{-2}	−0.06	< 0.001
0.3	−1.7	10^{-2}	−0.07	< 0.001
0.3	−1.8	10^{-0}	−0.01	< 0.001
0.3	−1.8	10^{-0}	−0.02	< 0.001
0.3	−1.8	10^{-0}	−0.03	< 0.001

Table 1—Continued

t	α	L_{min} (L_*)	γ_* (dex kpc $^{-1}$)	P_{KS}^a
0.3	−1.8	10^{-0}	−0.04	< 0.001
0.3	−1.8	10^{-0}	−0.05	0.003
0.3	−1.8	10^{-0}	−0.06	0.062
0.3	−1.8	10^{-0}	−0.07	0.002
0.3	−1.8	10^{-1}	−0.01	< 0.001
0.3	−1.8	10^{-1}	−0.02	< 0.001
0.3	−1.8	10^{-1}	−0.03	0.008
0.3	−1.8	10^{-1}	−0.04	0.077
0.3	−1.8	10^{-1}	−0.05	0.008
0.3	−1.8	10^{-1}	−0.06	< 0.001
0.3	−1.8	10^{-1}	−0.07	< 0.001
0.3	−1.8	10^{-2}	−0.01	< 0.001
0.3	−1.8	10^{-2}	−0.02	< 0.001
0.3	−1.8	10^{-2}	−0.03	< 0.001
0.3	−1.8	10^{-2}	−0.04	< 0.001
0.3	−1.8	10^{-2}	−0.05	< 0.001
0.3	−1.8	10^{-2}	−0.06	< 0.001
0.3	−1.8	10^{-2}	−0.07	< 0.001
0.4	−1.6	10^{-0}	−0.01	< 0.001
0.4	−1.6	10^{-0}	−0.02	< 0.001
0.4	−1.6	10^{-0}	−0.03	< 0.001
0.4	−1.6	10^{-0}	−0.04	0.084
0.4	−1.6	10^{-0}	−0.05	0.111
0.4	−1.6	10^{-0}	−0.06	< 0.001
0.4	−1.6	10^{-0}	−0.07	< 0.001
0.4	−1.6	10^{-1}	−0.01	< 0.001
0.4	−1.6	10^{-1}	−0.02	< 0.001
0.4	−1.6	10^{-1}	−0.03	0.019
0.4	−1.6	10^{-1}	−0.04	0.948
0.4	−1.6	10^{-1}	−0.05	0.010
0.4	−1.6	10^{-1}	−0.06	< 0.001
0.4	−1.6	10^{-1}	−0.07	< 0.001
0.4	−1.6	10^{-2}	−0.01	< 0.001
0.4	−1.6	10^{-2}	−0.02	< 0.001
0.4	−1.6	10^{-2}	−0.03	0.247
0.4	−1.6	10^{-2}	−0.04	0.105

Table 1—Continued

t	α	L_{min} (L_*)	γ_* (dex kpc $^{-1}$)	P_{KS}^a
0.4	−1.6	10^{-2}	−0.05	< 0.001
0.4	−1.6	10^{-2}	−0.06	< 0.001
0.4	−1.6	10^{-2}	−0.07	< 0.001
0.4	−1.7	10^{-0}	−0.01	< 0.001
0.4	−1.7	10^{-0}	−0.02	< 0.001
0.4	−1.7	10^{-0}	−0.03	< 0.001
0.4	−1.7	10^{-0}	−0.04	0.016
0.4	−1.7	10^{-0}	−0.05	0.217
0.4	−1.7	10^{-0}	−0.06	< 0.001
0.4	−1.7	10^{-0}	−0.07	< 0.001
0.4	−1.7	10^{-1}	−0.01	< 0.001
0.4	−1.7	10^{-1}	−0.02	< 0.001
0.4	−1.7	10^{-1}	−0.03	0.101
0.4	−1.7	10^{-1}	−0.04	0.829
0.4	−1.7	10^{-1}	−0.05	0.015
0.4	−1.7	10^{-1}	−0.06	< 0.001
0.4	−1.7	10^{-1}	−0.07	< 0.001
0.4	−1.7	10^{-2}	−0.01	< 0.001
0.4	−1.7	10^{-2}	−0.02	0.078
0.4	−1.7	10^{-2}	−0.03	0.227
0.4	−1.7	10^{-2}	−0.04	0.006
0.4	−1.7	10^{-2}	−0.05	< 0.001
0.4	−1.7	10^{-2}	−0.06	< 0.001
0.4	−1.7	10^{-2}	−0.07	< 0.001
0.4	−1.8	10^{-0}	−0.01	< 0.001
0.4	−1.8	10^{-0}	−0.02	< 0.001
0.4	−1.8	10^{-0}	−0.03	< 0.001
0.4	−1.8	10^{-0}	−0.04	0.002
0.4	−1.8	10^{-0}	−0.05	0.238
0.4	−1.8	10^{-0}	−0.06	0.010
0.4	−1.8	10^{-0}	−0.07	< 0.001
0.4	−1.8	10^{-1}	−0.01	< 0.001
0.4	−1.8	10^{-1}	−0.02	< 0.001
0.4	−1.8	10^{-1}	−0.03	0.083
0.4	−1.8	10^{-1}	−0.04	0.473
0.4	−1.8	10^{-1}	−0.05	0.022

Table 1—Continued

t	α	L_{min} (L_*)	γ_* (dex kpc $^{-1}$)	P_{KS}^a
0.4	−1.8	10^{-1}	−0.06	< 0.001
0.4	−1.8	10^{-1}	−0.07	< 0.001
0.4	−1.8	10^{-2}	−0.01	0.150
0.4	−1.8	10^{-2}	−0.02	0.132
0.4	−1.8	10^{-2}	−0.03	0.006
0.4	−1.8	10^{-2}	−0.04	< 0.001
0.4	−1.8	10^{-2}	−0.05	< 0.001
0.4	−1.8	10^{-2}	−0.06	< 0.001
0.4	−1.8	10^{-2}	−0.07	< 0.001
0.5	−1.6	10^{-0}	−0.01	< 0.001
0.5	−1.6	10^{-0}	−0.02	< 0.001
0.5	−1.6	10^{-0}	−0.03	< 0.001
0.5	−1.6	10^{-0}	−0.04	0.509
0.5	−1.6	10^{-0}	−0.05	0.003
0.5	−1.6	10^{-0}	−0.06	< 0.001
0.5	−1.6	10^{-0}	−0.07	< 0.001
0.5	−1.6	10^{-1}	−0.01	< 0.001
0.5	−1.6	10^{-1}	−0.02	< 0.001
0.5	−1.6	10^{-1}	−0.03	< 0.001
0.5	−1.6	10^{-1}	−0.04	0.955
0.5	−1.6	10^{-1}	−0.05	< 0.001
0.5	−1.6	10^{-1}	−0.06	< 0.001
0.5	−1.6	10^{-1}	−0.07	< 0.001
0.5	−1.6	10^{-2}	−0.01	< 0.001
0.5	−1.6	10^{-2}	−0.02	< 0.001
0.5	−1.6	10^{-2}	−0.03	0.003
0.5	−1.6	10^{-2}	−0.04	0.857
0.5	−1.6	10^{-2}	−0.05	< 0.001
0.5	−1.6	10^{-2}	−0.06	< 0.001
0.5	−1.6	10^{-2}	−0.07	< 0.001
0.5	−1.7	10^{-0}	−0.01	< 0.001
0.5	−1.7	10^{-0}	−0.02	< 0.001
0.5	−1.7	10^{-0}	−0.03	< 0.001
0.5	−1.7	10^{-0}	−0.04	0.263
0.5	−1.7	10^{-0}	−0.05	0.024
0.5	−1.7	10^{-0}	−0.06	< 0.001

Table 1—Continued

t	α	L_{min} (L_*)	γ_* (dex kpc $^{-1}$)	P_{KS}^a
0.5	−1.7	10^{-0}	−0.07	< 0.001
0.5	−1.7	10^{-1}	−0.01	< 0.001
0.5	−1.7	10^{-1}	−0.02	< 0.001
0.5	−1.7	10^{-1}	−0.03	0.003
0.5	−1.7	10^{-1}	−0.04	0.945
0.5	−1.7	10^{-1}	−0.05	0.003
0.5	−1.7	10^{-1}	−0.06	< 0.001
0.5	−1.7	10^{-1}	−0.07	< 0.001
0.5	−1.7	10^{-2}	−0.01	< 0.001
0.5	−1.7	10^{-2}	−0.02	< 0.001
0.5	−1.7	10^{-2}	−0.03	0.021
0.5	−1.7	10^{-2}	−0.04	0.529
0.5	−1.7	10^{-2}	−0.05	< 0.001
0.5	−1.7	10^{-2}	−0.06	< 0.001
0.5	−1.7	10^{-2}	−0.07	< 0.001
0.5	−1.8	10^{-0}	−0.01	< 0.001
0.5	−1.8	10^{-0}	−0.02	< 0.001
0.5	−1.8	10^{-0}	−0.03	< 0.001
0.5	−1.8	10^{-0}	−0.04	0.091
0.5	−1.8	10^{-0}	−0.05	0.135
0.5	−1.8	10^{-0}	−0.06	< 0.001
0.5	−1.8	10^{-0}	−0.07	< 0.001
0.5	−1.8	10^{-1}	−0.01	< 0.001
0.5	−1.8	10^{-1}	−0.02	< 0.001
0.5	−1.8	10^{-1}	−0.03	0.019
0.5	−1.8	10^{-1}	−0.04	0.935
0.5	−1.8	10^{-1}	−0.05	0.009
0.5	−1.8	10^{-1}	−0.06	< 0.001
0.5	−1.8	10^{-1}	−0.07	< 0.001
0.5	−1.8	10^{-2}	−0.01	< 0.001
0.5	−1.8	10^{-2}	−0.02	< 0.001
0.5	−1.8	10^{-2}	−0.03	0.245
0.5	−1.8	10^{-2}	−0.04	0.105
0.5	−1.8	10^{-2}	−0.05	< 0.001
0.5	−1.8	10^{-2}	−0.06	< 0.001
0.5	−1.8	10^{-2}	−0.07	< 0.001

Table 1—Continued

t	α	L_{min} (L_*)	γ_* (dex kpc $^{-1}$)	P_{KS}^a
0.6	−1.6	10^{-0}	−0.01	< 0.001
0.6	−1.6	10^{-0}	−0.02	< 0.001
0.6	−1.6	10^{-0}	−0.03	< 0.001
0.6	−1.6	10^{-0}	−0.04	0.835
0.6	−1.6	10^{-0}	−0.05	< 0.001
0.6	−1.6	10^{-0}	−0.06	< 0.001
0.6	−1.6	10^{-0}	−0.07	< 0.001
0.6	−1.6	10^{-1}	−0.01	< 0.001
0.6	−1.6	10^{-1}	−0.02	< 0.001
0.6	−1.6	10^{-1}	−0.03	< 0.001
0.6	−1.6	10^{-1}	−0.04	0.884
0.6	−1.6	10^{-1}	−0.05	< 0.001
0.6	−1.6	10^{-1}	−0.06	< 0.001
0.6	−1.6	10^{-1}	−0.07	< 0.001
0.6	−1.6	10^{-2}	−0.01	< 0.001
0.6	−1.6	10^{-2}	−0.02	< 0.001
0.6	−1.6	10^{-2}	−0.03	< 0.001
0.6	−1.6	10^{-2}	−0.04	0.814
0.6	−1.6	10^{-2}	−0.05	< 0.001
0.6	−1.6	10^{-2}	−0.06	< 0.001
0.6	−1.6	10^{-2}	−0.07	< 0.001
0.6	−1.7	10^{-0}	−0.01	< 0.001
0.6	−1.7	10^{-0}	−0.02	< 0.001
0.6	−1.7	10^{-0}	−0.03	< 0.001
0.6	−1.7	10^{-0}	−0.04	0.701
0.6	−1.7	10^{-0}	−0.05	< 0.001
0.6	−1.7	10^{-0}	−0.06	< 0.001
0.6	−1.7	10^{-0}	−0.07	< 0.001
0.6	−1.7	10^{-1}	−0.01	< 0.001
0.6	−1.7	10^{-1}	−0.02	< 0.001
0.6	−1.7	10^{-1}	−0.03	< 0.001
0.6	−1.7	10^{-1}	−0.04	0.955
0.6	−1.7	10^{-1}	−0.05	< 0.001
0.6	−1.7	10^{-1}	−0.06	< 0.001
0.6	−1.7	10^{-1}	−0.07	< 0.001
0.6	−1.7	10^{-2}	−0.01	< 0.001

4. Discussion

Although equations 1,2,3, and 7 include a significant number of free parameters, we emphasize that the GRB-DLA results, in particular, are sensitive to only a few of these relations. For the GRB-DLA, the results depend on four parameters (and the assumption that L_{1700} traces the SFR): the faint-end slope α , the metallicity Z_* of an $L = L_*$ galaxy, the power-law exponent β of the metallicity/luminosity relation, and the minimum luminosity L_{min} of a star-forming galaxy relative to L_* . Both α and Z_* are reasonably well constrained by observations at $z \approx 3$. Although β is not strongly constrained at $z = 3$, there is evidence that the local value of 0.2 is also valid (Ledoux et al. 2006; Erb et al. 2006; Prochaska et al. 2007) (see also Fig. 4). Therefore, the GRB-DLA results are sensitive to only two relatively unconstrained parameters. Regarding L_{min} , assuming $\alpha \leq -1.6$ we find good agreement between observations and model for $L_{min} < 10^{-3}L_*$ and we cannot rule out $L_{min} \approx 10^{-2}L_*$. In terms of the metallicity/luminosity relation, we have not extensively explored β in part because there is degeneracy in the metallicity predictions between α and β .

The QSO-DLA models do include additional scaling laws and therefore more free parameters. Specifically, we have included a Holmberg relation and metallicity gradient for the gas in star-forming galaxies. Neither of these relations have been constrained observationally at high redshift (however, there is evidence that abundance gradients exist in some high- z galaxies, see Förster Schreiber et al. 2006); we assumed values from the local universe. We also note there is evidence for metallicity gradients in QSO-DLA galaxies at intermediate redshifts (Chen, Kennicutt & Rauch 2005). To this extent, we do not consider the results shown in Fig. 6 to be a special success. Nevertheless, our results demonstrate that the observations are reproduced when adopting standard values for these prescriptions from the local universe. One implication of this success is that the model may be a fair representation of average scaling relations that must be at place at $z \approx 3$. We wish to caution, however, that there is large degeneracy between the various relations applied for the QSO-DLA.

4.1. How biased are the QSO-DLA and GRB-DLA samples?

An obvious question is whether our QSO-DLA and GRB-DLA samples are representative of the underlying galaxy populations? It has long been discussed to which extent QSO-DLA samples are biased against dusty (and hence likely metal rich and/or large $\log N(\text{H I})$) systems. Studies of radio selected DLAs (free from dust-bias) have found similar column density and metallicity distributions as for optically selected DLA samples (Ellison et al. 2001, 2004; Ellison, Hall & Lira 2005; Akerman et al. 2005; Jorgenson et al. 2006) showing that any dust bias will be so small that it will not fundamentally change the conclusions

Table 1—Continued

t	α	L_{min} (L_*)	γ_* (dex kpc $^{-1}$)	P_{KS}^a
0.6	−1.7	10^{-2}	−0.02	< 0.001
0.6	−1.7	10^{-2}	−0.03	< 0.001
0.6	−1.7	10^{-2}	−0.04	0.910
0.6	−1.7	10^{-2}	−0.05	< 0.001
0.6	−1.7	10^{-2}	−0.06	< 0.001
0.6	−1.7	10^{-2}	−0.07	< 0.001
0.6	−1.8	10^{-0}	−0.01	< 0.001
0.6	−1.8	10^{-0}	−0.02	< 0.001
0.6	−1.8	10^{-0}	−0.03	< 0.001
0.6	−1.8	10^{-0}	−0.04	0.501
0.6	−1.8	10^{-0}	−0.05	0.002
0.6	−1.8	10^{-0}	−0.06	< 0.001
0.6	−1.8	10^{-0}	−0.07	< 0.001
0.6	−1.8	10^{-1}	−0.01	< 0.001
0.6	−1.8	10^{-1}	−0.02	< 0.001
0.6	−1.8	10^{-1}	−0.03	< 0.001
0.6	−1.8	10^{-1}	−0.04	0.952
0.6	−1.8	10^{-1}	−0.05	< 0.001
0.6	−1.8	10^{-1}	−0.06	< 0.001
0.6	−1.8	10^{-1}	−0.07	< 0.001
0.6	−1.8	10^{-2}	−0.01	< 0.001
0.6	−1.8	10^{-2}	−0.02	< 0.001
0.6	−1.8	10^{-2}	−0.03	0.003
0.6	−1.8	10^{-2}	−0.04	0.859
0.6	−1.8	10^{-2}	−0.05	< 0.001
0.6	−1.8	10^{-2}	−0.06	< 0.001
0.6	−1.8	10^{-2}	−0.07	< 0.001

^aProbability from KS test analysis.

about cross-section and metallicity distributions inferred from optically selected surveys.

Concerning GRB-DLA there is no dust bias in the detection of the prompt emission itself as γ -rays are unaffected by dust. However, the requirement of an optical afterglow detection from which the redshift the H I column density and metal columns can be measured does potentially exclude very dusty sightlines. Furthermore, there could be an intrinsic (astrophysical) bias against high metallicity in GRB production. In the collapsar model the limit is estimated to be around $0.3 Z_{\odot}$ (Hirschi et al. 2005; Woosley & Heger 2005), but this is very dependent on the as yet poorly understood properties of winds from massive stars (e.g. clumping, Smith 2007). We also note that Wolf & Podsiadlowski (2007) exclude a metallicity cut-off below half the solar value based on statistics of host galaxy luminosities. If true such an intrinsic bias could preferentially exclude massive, dust-obscured starbursts, that typically seem to be enriched above this limit (Swinbank et al. 2004), from the GRB samples. Nevertheless, a few extremely red and luminous GRB hosts have been found (Levan et al. 2006; Berger et al. 2007). So far there are few examples of GRB sightlines with very large dust columns (for recent examples see Rol et al. 2007; Jaunsen et al. 2008; Tanvir et al. 2008). The near, mid and far-IR properties of GRB host galaxies have been studied by a number of groups (e.g., Chary et al. 2002; Le Floc'h et al. 2003, 2006; Berger et al. 2003; Tanvir et al. 2004; Priddey et al. 2006; Castro Cerón et al. 2007). A few GRB hosts, all at $z < 2$, have tentatively been detected at sub-mm wavelengths, but their inferred UV/optical (bluer, Gorosabel et al. 2003a,b) and dust properties (higher temperatures, Michałowski et al. 2008) are different than those of sub-mm selected galaxies.

We are currently in the process of building up a γ -ray/X-ray selected sample of GRBs with the aim of getting control on the issue of bias (Jakobsson et al. 2006b; Fynbo et al. in preparation). Our sample selection excludes bursts with high foreground extinction and low sun angle. Hence, the sample includes bursts for which conditions for optical follow-up are favourable, but the sample is not biased towards optically bright bursts. Currently, optical afterglows are detected for about 80% of the bursts in our sample and there is no obvious difference in the X-ray absorption properties of GRBs with and without detected optical afterglows. Therefore, we consider it unlikely that the current sample of GRB-DLA is strongly biased against high metallicity and dusty systems, but this is an issue that still needs to be clarified. In terms of the analysis presented here, we conclude that dust bias will play a minor role.

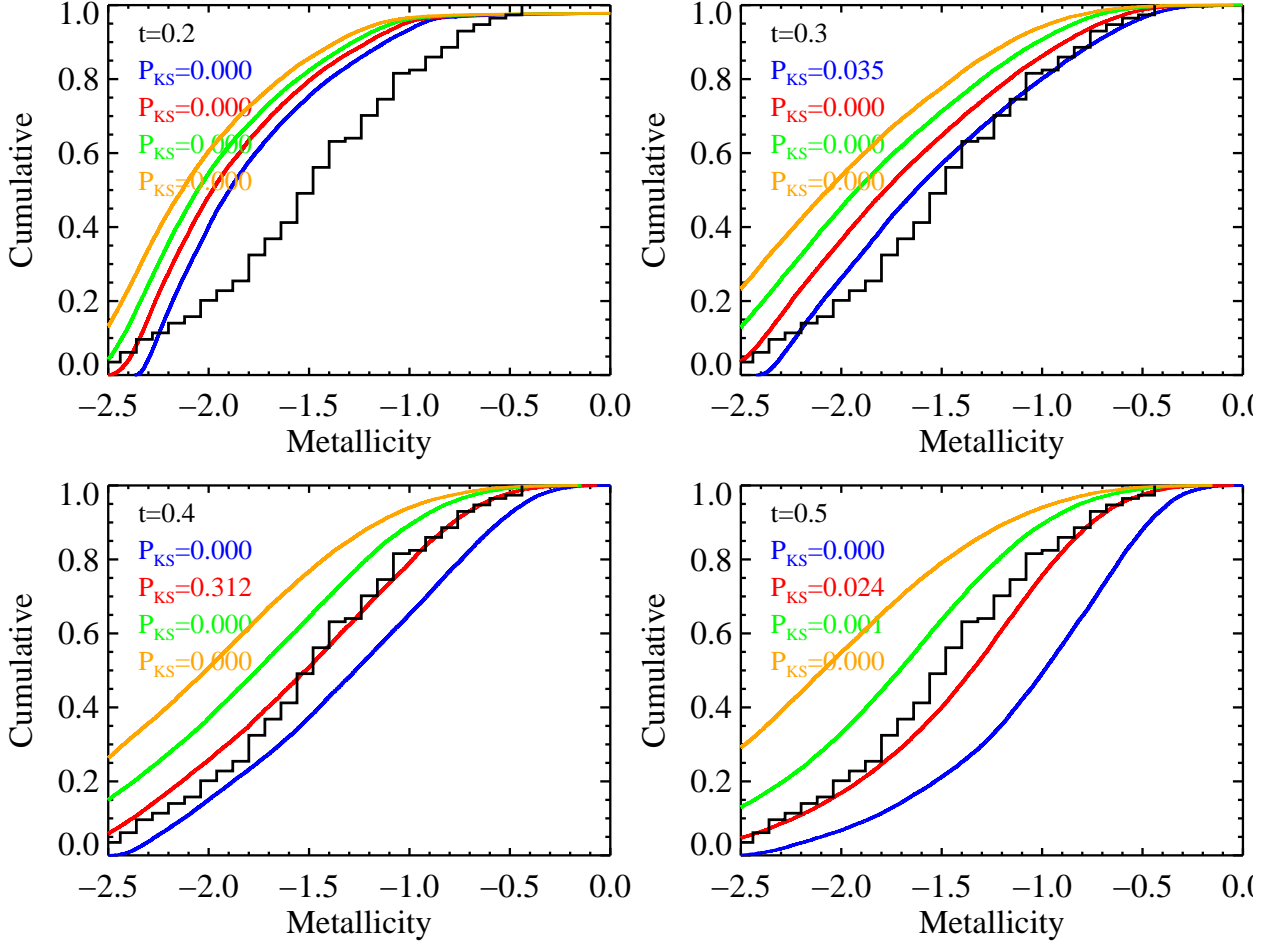


Fig. 6.— The histograms show the cumulative distribution of QSO-DLA metallicities. The four panels show the predicted metallicity distribution in our simple model assuming values of t ranging from 0.2 to 0.5. For each assumed value of t we plot the model for values of γ_* (in units of dex kpc $^{-1}$) of -0.07 (orange), -0.05 (green), -0.03 (red), and -0.01 (blue). For each model we derive the probability of a KS test comparing the model to the data. Holmberg slopes of $t = 0.3$ – 0.5 and radial abundance gradients of $\gamma_* = 0.01$ – 0.05 dex kpc $^{-1}$ provide acceptable fits. For all models shown here we have used $\alpha = -1.7$ and $L_{min} = 0.0001 L_*$.

4.2. How can this simple picture be tested?

The best fitting model has a value of the Holmberg parameter t of 0.4. For $t = 0.5$, the probability to select a GRB host or a DLA galaxy counterpart with luminosity L is identical in our model. For values of t less than 0.5, QSO-DLA galaxies counterparts are predicted to be on average fainter than GRB host galaxies. An indication that this indeed may be the case comes from the fact that $\text{Ly}\alpha$ emission is detected more often in GRB-DLA than QSO-DLA. However, this may also be a result of the on average smaller impact parameters for GRB sightlines and the fact the GRB hosts are probably selected to have a high instantaneous specific star-formation rate.

One way to test this model is to measure the luminosities of GRB and QSO-DLA selected galaxies and compare with the predictions of the model. Unfortunately, it has proven extremely difficult to detect QSO-DLA galaxy counterparts in emission to the glare of the bright background QSOs. However, a clear prediction of the model (see Fig. 3) is that the most metal rich QSO-DLA should have the brightest galaxy counterparts and the largest impact parameters. It would therefore be interesting to target a sample of such DLAs and constrain the statistical properties of the galaxy counterparts.

The outlook for a statistically significant sample of GRB host galaxy luminosities is much better (Hjorth et al. 2008, in preparation). In Jakobsson et al. (2005) it is described how the model can be tested from a sample of GRB host galaxy luminosities and upper limits. Given the heterogeneous nature of the current sample of GRB-DLA with metallicity measurements it is also important to obtain metallicity measurements for a more complete sample of GRB-DLA. Instruments like the X-shooter spectrograph on the European Southern Observatory Very Large Telescope will make this feasible in the near future (Kaper et al. 2008).

5. Conclusions

We find that with a simple model including the luminosity function for LBGs, a Holmberg relation for $\sigma(L)$, an L-Z relation and a metallicity gradient with a slope γ dependent on luminosity it is possible to reconcile the metallicity distributions of QSO-DLA, GRB-DLA and LBGs. In this model the faint end of the luminosity function plays a very important role. As seen in the lower panel in Fig. 3 more than 75% of star-formation selected galaxies are fainter than the flux limit for LBGs, $R=25.5$. For QSO-DLA galaxies the fraction is even higher. Hence, in this model the GRB and DLA samples, in contrast with magnitude limited surveys, provide an almost complete census of $z \approx 3$ star-forming galaxies that are

not heavily obscured.

We acknowledge helpful discussions with E. Ramirez-Ruiz and M. Pettini, Andrew Pontzen, and H.-W. Chen. We also thank the anonymous referee for a very constructive and helpful report. J. X. P. is partially supported by NASA/Swift grants NNG06GJ07G and NNX07AE94G and an NSF CAREER grant (AST-0548180). This research was supported by the DFG cluster of excellence “Origin and structure of the Universe”. The Dark Cosmology Centre is funded by the DNRF.

REFERENCES

- Adelberger, K. L., & Steidel, C. C. 2000, *ApJ*, 544, 218.
- Akerman, C. J., Ellison, S. L., Pettini, M., & Steidel, C. C. 2005, *A&A*, 440, 499.
- Baldry, I. K., Glazebrook, K., Budavári, T., et al. 2005, *MNRAS*, 358, 441.
- Berger, E., Kulkarni, S. R., Bloom, J. S., et al. 2002, *ApJ*, 581, 981.
- Berger, E., Cowie, L. L., Kulkarni, S. R., et al. 2003, *ApJ*, 588, 99.
- Berger, E., Fox, D. B., Kulkarni, S. R., et al. 2007, *ApJ*, 660, 504.
- Blanton, M. R., Lupton, R. H., Schlegel, D. J., et al. 2005, *ApJ*, 631, 208.
- Bloom, J. S., Kulkarni, S. R., & Djorgovski, S. G. 2002, *AJ*, 123, 1111.
- Boisier, S., & Prantzos, N. 2001, *MNRAS*, 325, 321.
- Bowen, D. V., Jenkins, E. B., Pettini, M., & Tripp, T. M. 2005, *ApJ*, 635, 880.
- Bresolin, F., Garnett, D. R., & Kennicutt, R. C. 2004, *ApJ*, 615, 228.
- Castro Cerón, J. M., Michałowski, M. J., Hjorth, J., et al. 2007, *ApJ*, 653, L85.
- Chapman, S. C., Blain, A. W., Smail, I., & Ivison, R. J., 2005, *ApJ*, 622, 772.
- Chary, R., Becklin, E. E., & Armus, L. 2002, *ApJ*, 566, 229.
- Chen, H.-W., Lanzetta, K. M., & Fernandez-Soto, A. 2000, *ApJ*, 533, 120.
- Chen, H.-W., & Lanzetta, K. M. 2003, *ApJ*, 597, 706.

- Chen, H.-W., Kennicutt, R. C. Jr., & Rauch, M. 2005, *ApJ*, 620, 703.
- Christensen, L., Hjorth, J., Gorosabel, J. 2004, *A&A*, 425, 913.
- Cimatti, A., Daddi, E., Cassata, P., et al. 2003, *A&A*, 412, L1.
- Dekel, A. and Woo, J. 2003, *MNRAS*, 344, 1131.
- Ellison, S. L., Yan, L., Hook, I. M., et al. 2001, *A&A*, 379, 393.
- Ellison, S. L. Churchill, C. W., Rix, S. A., & Pettini, M. 2004, *ApJ*, 615, 118.
- Ellison, S. L., Hall, P. B., & Lira, P. 2005, *AJ*, 130, 1345.
- Erb, D. K., Shapley, A. E., Pettini, M., et al. 2006, *ApJ*, 644, 813.
- Feigelson, E. D. and Nelson, P. I. 1985, *ApJ*, 293, 192.
- Fernández-Soto, A., Lanzetta, K. M., & Yahil, A. 1999, *ApJ*, 513, 34.
- Förster Schreiber, N. M., Genzel, R., Lehnert, M. D., et al. 2006, *ApJ*, 645, 1062.
- Fruchter, A. S., Levan, A., Strolger, L., et al. 2006, *Nature*, 441, 463.
- Fynbo, J. U., Møller, P., & Warren, S. J. 1999, *MNRAS*, 305, 849.
- Fynbo, J. P. U., Ledoux, C., Møller, P., et al. 2003, *A&A*, 407, 147.
- Fynbo, J. P. U., Watson, D., Thöne, C. C., et al. 2006a, *Nature*, 444, 1047.
- Fynbo, J. P. U., Starling, R. L. C., Ledoux, C., et al. 2006b, *A&A*, 451, L47.
- Gorosabel, J., Christensen, L., Hjorth, J. et al. 2003a, *A&A*, 400, 127.
- Gorosabel, J., Klose, S., Christensen, L., et al. 2003b, *A&A*, 409, 123.
- Hammer, F. *et al.* 2006, *A&A*, 454, 103.
- Hirschi, R., Meynet, G., & Maeder, A. 2005, *A&A*, 443, 581.
- Hjorth, J., Møller, P., Gorosabel, J., et al. 2002, *ApJ*, 597, 699.
- Hjorth, J., Sollerman, J., Møller, P., et al. 2003, *Nature*, 423, 847.
- Hogg, D. W., & Fruchter, A. S. 1999, *ApJ*, 520, 54.
- Hu, E. M., Cowie, L., & McMahon, R. G. 1998, *ApJ*, 502, L99.

- Hughes, D. H., Serjeant, S., Dunlop, J., et al. 1998, *Nature*, 394, 241.
- Jakobsson, P., Björnsson, G., Fynbo, J. P. U., et al. 2005, *MNRAS*, 362, 245.
- Jakobsson, P., Fynbo, J. P. U., Ledoux, C., et al. 2006, *A&A*, 460, L13.
- Jakobsson, P., Levan, A., Fynbo, J. P. U., et al. 2006, *A&A*, 447, 849.
- Jaunsen, A. O., Rol, E., Watson, D. J., et al. 2008, *ApJ*, in press (arXiv:0803.4017).
- Jerjen, H., Tully, B., & Trentham, N. 2004, *PASA*, 21, 356.
- Jorgenson, R. A., Wolfe, A. M., Prochaska, J. X., et al. 2006, *ApJ*, 646, 730.
- Kaper, L., D’Odorico, S., Hammer, F., Pallavicini, R., & Kjaergaard Rasmussen, P. 2008, To appear in Proceedings ESO workshop on ”Science with the VLT in the E-ELT era”, Ed. A. Moorwood.
- Kennicutt, R. C. 1998, *ARA&A*, 36, 189.
- Kobulnicky, H. A. and Kewley, L. J. 2004, *ApJ*, 617, 240.
- Ledoux, C., Petitjean, P., Fynbo, J. P. U., Møller, P., & Srianand, R. 2006, *A&A*, 457, 71.
- Le Floch, E., Duc, P.-A., Mirabel, I. F. 2003, *A&A*, 400, 499.
- Le Floch, E., Charmandaris, V., Forrest, W. J., et al. 2006, *ApJ*, 642, 636.
- Levan, A. J., Fruchter, A. S., Rhoads, J., et al. 2006, *ApJ*, 647, 471.
- Magrini, L., Vílchez, J. M., Mampaso, A., Corradi, R. L. M., & Leisy, P. 2007, *A&A*, 470, 865.
- Mateo, M. L. 1998, *ARA&A*, 36, 435.
- Michałowski, M. J, Hjorth, J., Castro Cerón, J. M., Watson, D. 2008, *ApJ*, 672, 817.
- Miley, G., & De Breuck, C. 2008, *A&ARv*, 15, 67.
- Møller, P., Fynbo, J. P. U., & Fall, S. M., 2004, *A&A*, 422, L33.
- Møller, P., Warren, S. J., Fall, S. M., Fynbo, J. U., & Jakobsen, P. 2002, *ApJ*, 574, 51.
- Pettini, M., Shapley, A. E., Steidel, C. C., et al. 2001, *ApJ*, 554, 981.
- Pettini, M., Rix, S. A., Steidel, C. C., et al. 2002, *ApJ*, 569, 742.

- Priddey, R. S., Tanvir, N. R., Levan, A. J., et al. 2006, MNRAS, 369, 1189.
- Prochaska, J. X. et al. 2003, ApJ, 595, L9.
- Prochaska, J. X., Herbert-Fort, S., and Wolfe, A. M. 2005, ApJ, 635, 123.
- Prochaska, J. X. 2006, ApJ, 650, 272.
- Prochaska, J. X., Chen, H.-W., Bloom, J. S. 2006, ApJ, 648, 95.
- Prochaska, J. X., Chen, H.-W., Dessauges-Zavadsky, M., & Bloom, J. S. 2007, ApJ, 666, 267.
- Rauch, M., Haehnelt, M., Bunker, A., et al. 2007, ApJ, in press (arXiv:0711.1354).
- Reddy, N. A., Erb, D. K., Steidel, C. C., et al. 2005, ApJ, 633, 748.
- Reddy, N. A., Steidel, C. C., Pettini, M., et al. 2008, ApJS, 175, 48.
- Rol, E., van der Horst, A., Wiersema, K., et al. 2007 ApJ, 669, 1098.
- Savaglio, S., Glazebrook, K., Le Borgne, D., et al. 2005, ApJ, 635, 260.
- Savaglio, S., NJPh, 8, 195.
- Schulte-Ladbeck, R. E., Köning, B., Miller, J. J., et al. 2005, ApJ, 625, L79.
- Smartt, S. J., & Rolleston, W. R. J. 1997, ApJ, 481, L47.
- Smith, N. 2007, arXiv:0710.3430.
- Sommer-Larsen, J., & Fynbo, J. P. U. 2008, MNRAS, 385, 3.
- Stanek, K. Z., Matheson, T., Garnavich, P. M., et al. 2003, ApJ, 591, L17.
- Steidel, C. C., Adelberger, K. L., Shaplet, A. E., et al. 2003, ApJ, 592, 728.
- Swinbank, A. M., Smail, I., Chapman, S. C., et al. 2004, ApJ, 617, 64.
- Tanvir, N. R., Barnard, V. E., Blain, A. W., et al. 2004, MNRAS, 352, 1073.
- Tanvir, N. R., Levan, A. J., Rol, E., et al. 2008, MNRAS, submitted (arXiv:0803.4100).
- Tremonti, C. A., Heckman, T. M., Kauffmann, G., et al. 2004, ApJ, 613, 898.
- van Dokkum, P. G., Quadri, R., Marchesini, D., et al. 2006, ApJ, 638, L59.

- Williams, R. E., Blacker, B., Dickinson, M., et al. 1996, *AJ*, 112, 1335.
- Wolf, C., & Podsiadlowski, P. 2007, *MNRAS*, 375, 1049.
- Wolfe, A. M. et al. 1986, *ApJS*, 61, 249.
- Wolfe, A. M., Gawiser, E., & Prochaska, J. X. 2003, *ApJ*, 593, 235.
- Wolfe, A. M., Ouk, J. C., Gawiser, E., Prochaska, J. X., & Lopez, S. 2004, *ApJ*, 615, 625.
- Wolfe, A. M., Gawiser, E., & Prochaska, J. X. 2005, *ARA&A*, 43, 861.
- Woosley, S. E., & Heger, A. 2006, *ApJ*, 637, 914.
- Zwaan, M., van der Hulst, J. M., Briggs, F. H., et al. 2005, *MNRAS*, 364, 1467.